Storm-induced circulation in the Pearl River Estuary of China during super Typhoon Koryn

Liqun Tang, Jinyu Sheng and Yuhan Cai

ABSTRACT

This study presents a numerical investigation of storm-induced circulation and hydrographic distributions over the Pearl River Estuary (PRE) in South China's Guangdong Province during super Typhoon Koryn in June 1993. The nested-grid modelling system used in this study has three downscaling subcomponents: an outer-most sub-model with a coarse horizontal resolution of ~7 km for simulating surface elevations and depth-mean currents forced by wind and tides over China Seas from Bohai Sea to the northern South China Sea; and an inner-most sub-model with a fine resolution of ~1.2 km for simulating the three-dimensional estuarine circulation and hydrographic distributions in the PRE and adjacent waters. A parametric vortex is inserted into the coarse-resolution (0.5°) numerical weather forecast products to better represent the atmospheric pressure and wind stress associated with Koryn. Model results demonstrate that large surface elevations and intense surface currents are generated over the area of influence of the storm. Lagrange velocities of near-surface particles are also used to examine the effect of the storm on the movements and dispersion of near-surface particles over the study region.

Key words | particle trajectories, Pearl River Estuary, storm-induced circulation, storm surge, Typhoon Koryn

Liqun Tang
Department of Sediment Research,
China Institute of Water Resources and Hydropower Research,
Beijing,
China

Jinyu Sheng (corresponding author)
Department of Oceanography,
Dalhousie University,
Nova Scotia,
Canada,
B3H 4J1
E-mail: *Jinyu.Sheng@Dal.Ca*

Yuhan Cai
A9.com Inc,
130 Lytton Ave,
Palo Alto,
CA,
USA,
94301

INTRODUCTION

Circulation and hydrography over many shelf seas and coastal waters, such as the eastern Canadian continental shelf, Atlantic and Gulf waters of the United States, and coastal waters in South and Southeast Asia, are subject to tropical storms and hurricanes (or typhoons). The coastal ecosystems, which are highly sensitive to variations in circulation and hydrographic distributions, are under multiple stresses due to the combined effect of human development over the coastal zones and climate change. Better knowledge of the oceanographic response of the shelf and coastal waters to storms and hurricanes is needed in order to have effective management of natural resources over the shelf and coastal waters.

The Pearl River Estuary (PRE) in the east of the Pearl River Delta (PRD) of South China is a subtropical estuary with a surface area of $\sim 2.5 \times 10^3$ km^2. The estuary connects the Pearl River with the South China Sea. The Pearl River is the largest river system in Southern China, with an annual mean discharge of $\sim 3.36 \times 10^{11}$ m^3. The PRD occupies the low-lying areas alongside the PRE with a population of ~50 million people. The delta is rich in agriculture and aquaculture resources. The PRD has been in the forefront of the economic expansion in the last 30 years. Rapid urbanization and industrialization of this region with influxes of people from other parts of China have brought serious deterioration of the water quality in the PRE (Harrison *et al.* 2008). Pollutants such as inorganic nitrogen, active phosphate and petroleum hydrocarbons have resulted in a high number of harmful algae blooms in the PRE. The harmful algal blooms in the PRE during March–April 1998, for an example, caused economic losses estimated to be over US$45 million (Wang *et al.* 2008). Hydrodynamics play a very important role in affecting water quality and ecosystem dynamics in the PRE. Reliable information on the

doi: 10.2166/wqrjc.2012.111

three-dimensional (3D) circulation and capability of predicting circulation are required for better management of water quality and coastal resources over this region.

The general circulation and hydrographic distributions in the PRE are affected by many forcing mechanisms including tides, wind, sea surface heat and freshwater fluxes, and buoyancy forcing associated with freshwater runoff from the Pearl River system. Significant efforts have been made to examine the general hydrographic features and main physical processes in the estuary (Wong *et al.* 2003a, b; Larson *et al.* 2005; Harrison *et al.* 2008; Gan *et al.* 2009). Tang *et al.* (2009) and Ji *et al.* (2011a, b) recently examined the main physical processes affecting the general circulation and associated synoptic and seasonal variability of the estuarine circulation in the PRE using a nested-grid coastal ocean circulation model with large-scale atmospheric forcing fields and tides.

The PRE has also frequently been under threat from natural hazards such as typhoons and storm surges (Huang *et al.* 2004). Zhao *et al.* (2009) investigated phytoplankton blooms near the PRE induced by Category 2 Typhoon Nuri in August 2008 based on remotely sensing and *in situ* observations. They demonstrated the important role of increased river runoff, mixing and upwelling associated with the storm in generating the nearshore and offshore phytoplankton blooms. Nevertheless, inadequate understanding of main physical processes affecting the circulation and hydrography in the PRE during storms limits our ability to accurately predict the effect of the storm on the physical and biological environments in the region. The main objective of this study is to examine the storm-induced circulation during super Typhoon Koryn in the PRE and adjacent waters. Super Typhoon Koryn is selected in this study since it was a powerful super Typhoon that made a landfall near the PRE and affected significantly the ecosystem dynamics in the PRE and adjacent waters.

Koryn was the first typhoon during the Pacific typhoon season in 1993 and formed near the Caroline Islands on June 15 as a low pressure system. Koryn moved northward and then westward, and became a tropical storm on June 17 (Figure 1). By June 23, Koryn had strengthened to a typhoon status, with a maximum sustained wind speed of 120 km h^{-1}. The storm rapidly intensified in the next 24 h and became the first super typhoon of the season with winds of 225 km h^{-1} and a minimal pressure of 910 mbar. After making a landfall on the east coast of northern Luzon in the northern Philippines on June 26, with the maximum winds estimated at 210 km h^{-1}, Koryn entered the South China Sea as a Category 2 typhoon around noon on June 26. It then moved rapidly west-northwest across the northern part of the South China Sea with winds of 165 km h^{-1}. Koryn then slowly wound down, bringing heavy rain through China and northern Vietnam. After landfall to the southeast of the PRE, the storm dissipated on June 28. The main focus of this study is on the hydrodynamic responses of the PRE and adjacent waters to Koryn.

The arrangement of this paper is as follows: the next section provides the nested-grid coastal ocean model setup and forcing, which is followed by a discussion of the storm-induced circulation in the PRE and adjacent waters, and finally a summary and conclusion.

CIRCULATION MODEL SETUP AND EXTERNAL FORCING

The ocean circulation model used in this study is a nested-grid coastal ocean modelling system developed for the PRE (DalCoast-PRE) by Sheng *et al.* (2009a) and Tang *et al.* (2009) based on the Princeton Ocean Model (POM; Mellor 2004). DalCoast-PRE has three downscaling components (Figure 2): (a) an outer model with the domain covering the China Seas from Bohai Sea to the northern South China Sea; (b) a middle model with the domain covering the inner shelf of the northern South China Sea; and (c) an inner model with the domain covering the PRE and the adjacent waters. The outer model has a horizontal resolution of ~7 km. The middle model is nested inside the outer model domain and has a horizontal resolution of ~3 km. The inner model is nested inside the middle model domain and has a horizontal resolution of ~1.2 km. The outer model simulates surface elevations and depth-mean currents driven by wind forcing and tides. Both the middle and inner models simulates the 3D circulation and hydrography. This nested-grid modelling system has an advantage over other numerical models developed previously for the PRE since the outer model provides dynamically reliable information of tidal and large-scale

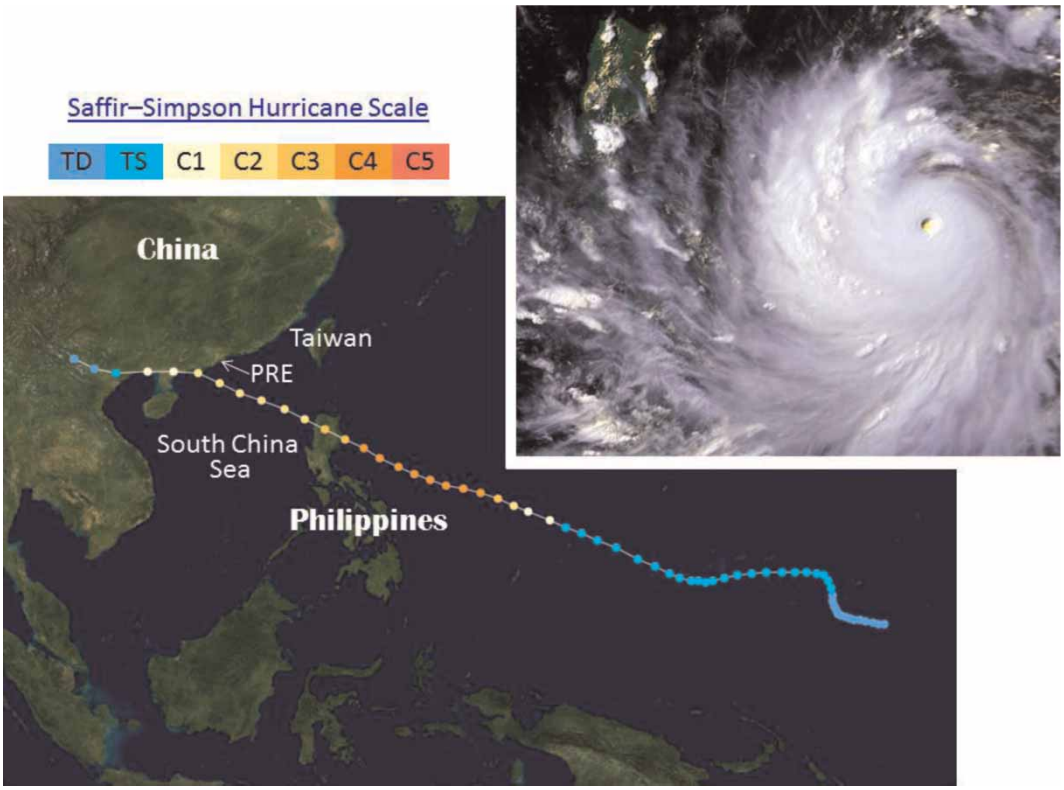

Figure 1 | The storm track (colored dots) of Typhoon Koryn from June 13 to 28, 1993 at a time interval of 3 h. The intensity of the storm is represented by the colors of the dots. Abbreviations in the color bar for the storm intensity (in Saffir-Simpson Hurricane Scale) are used for Tropical Depression (TD), Tropical Storm (TS), and Categories 1–5 (C1-C5). The inset shows the satellite cloud image of Koryn at 07:44 on June 24, 1993. Please refer to the online version of this paper to see this figure in colour: http://www.iwaponline.com/wqrjc/toc.htm.

wind-driven oceanic circulations for open boundary conditions of the middle and inner models in simulating the 3D coastal and estuarine circulations in the PRE and adjacent areas.

DalCoast-PRE is driven by time-dependent and spatially varying forcing functions including tidal and atmospheric forcing, and buoyancy forcing associated with river discharges. The tidal forcing used in this study is tidal elevations specified along the open boundaries of the outer model based on 16 pre-calculated tidal constituents (i.e., M_2, S_2, N_2, K_2, $2N_2$, μ_2, ν_2, L_2, T_2, K_1, O_1, P_1, M_1, OO_1, and J_1; see Matsumoto *et al.* 2001) using the tidal boundary condition of Davies & Flather (1978). Through the one-way nesting, the tides affect the circulation in the middle and inner models. The atmospheric forcing for the three components of the nested-grid system includes the sea level atmospheric pressure (SLP) and surface wind stress, taken from 3-hourly numerical weather forecast fields with a horizontal resolution of 0.5° (~50 km in the PRE) produced by the National Marine Environmental Forecast Center of China (NMEFC). Since the NMEFC fields do not resolve well the horizontal structure of wind and atmospheric pressure fields inside typhoons, a parametric vortex was inserted to the NMEFC fields based on the idealized wind and pressure profiles in typhoons and hurricanes suggested by Holland (1980):

$$p_s(r) = p_c + (p_n - p_c)\exp(-A/r^B) \tag{1}$$

$$V_s(r) = \left[AB(p_n - p_c)\exp(-A/r^B)/\rho_a r^B + r^2 f^2/4\right]^{1/2} - rf/2 \tag{2}$$

where $p_s(r)$ and $V_s(r)$ are the atmospheric pressure at the sea level and the (gradient) wind speeds at radius r, respectively, with respect to the storm center at (x_c, y_c), p_n is the ambient pressure, p_c is the atmospheric pressure at the storm center,

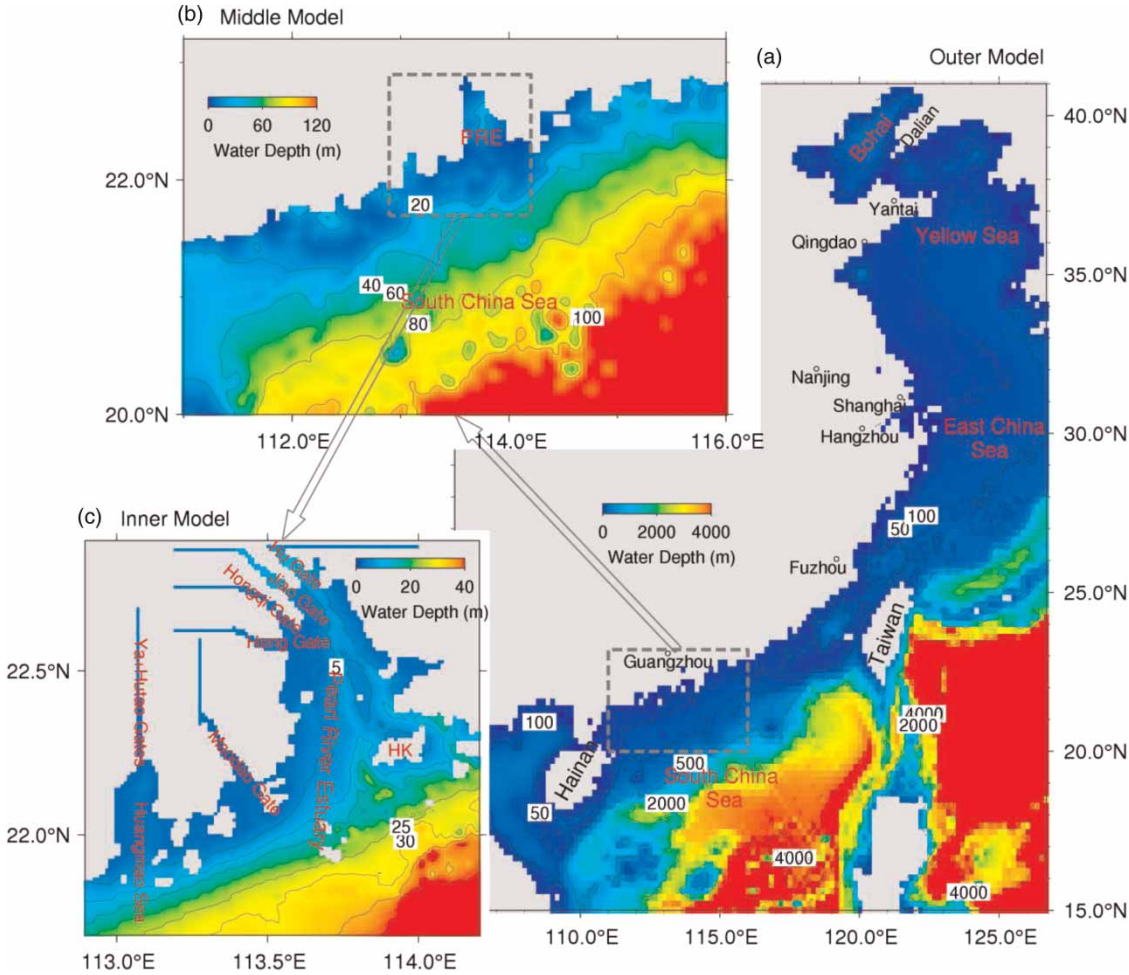

Figure 2 | Major bathymetric features of the nested-grid coastal ocean circulation modelling system for the Pearl River Estuary based on the Princeton Ocean Model (POM). (a) The outer model is a coarse-resolution (~7 km) storm surge model; (b) the middle model is an intermediate-resolution (~3 km) shelf circulation baroclinic model for the inner shelf of the northern South China Sea; (c) the inner model is a fine-resolution (~1.2 km) coastal circulation model for the Pearl River Estuary (PRE) and adjacent waters.

f is the Coriolis parameter, and ρ_a is the air density (assumed constant at 1.15 kg m^{-3}). In the above equations, A and B are two scaling parameters determined by

$$A = R_m^B, \quad B = \left(\frac{V_m}{p_n - p_c}\right)^2 \left(\frac{1}{\rho_a e}\right) \tag{3}$$

where V_m is the maximum wind speed at the radius of $r = R_m$. In this study, time series of the storm center position (x_c, y_c), the maximum wind speed (V_m), center (p_c) and ambient (p_n) atmospheric pressures for Typhoon Koryn were taken from the best track dataset for tropical cyclones in the western North Pacific constructed by the Shanghai Typhoon Institute (www.typhoon.gov.ca). Since the best track dataset does not contain R_m, its values for super Typhoon Koryn were estimated from the atmospheric pressure at the storm center (p_c) and the maximum wind speed (V_m) using the empirical formula suggested by Song (2003). In the model integration, the above parametric wind and atmospheric pressure profiles were calculated at each model time step and then inserted onto the interpolated NMEFC fields.

Figure 3 presents snapshots of wind stress and atmospheric pressure fields from 18:00 June 25 to 06:00 June 27 (Coordinated Universal Time, UTC) based on the combination of the large-scale atmospheric fields produced by the National Marine Environmental Forecast Center and Holland's parametric vortex. The parametric atmospheric

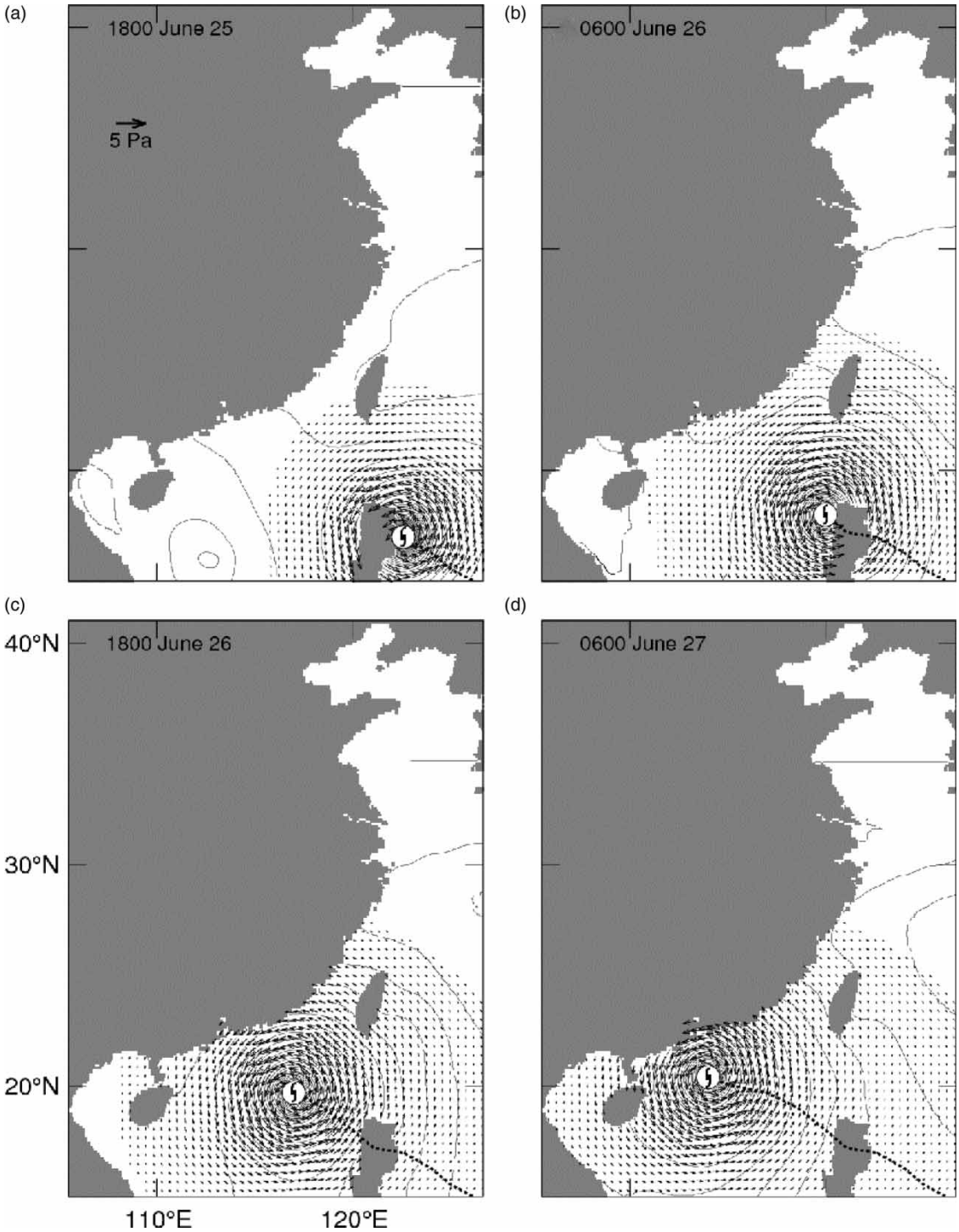

Figure 3 | Snapshots of wind stress (vectors) and atmospheric pressures during Typhoon Koryn at (a) 18:00 June 25, (b) 06:00 June 26, (c) 18:00 June 26, and (d) 06:00 June 27, 1993.

pressure and wind fields for Typhoon Koryn are nearly symmetric with respect to the center of the storm, which resemble reasonably well the general features of super Typhoon Koryn in the deep waters before making landfall (Figures 3(b),(c)). The storm became asymmetric once it reached the coastal waters and started to make landfall

(Figure 1). The parametric vortex shown in Figure 3(d), however, does not to represent well the asymmetric feature of the storm, indicating that a more realistic hurricane model is needed during the landfall of the storm.

The middle and inner models of the nested-grid modelling system are also forced by the buoyancy forcing associated with the surface heat flux (calculated using the bulk formulae discussed in Gill (1982)) and freshwater discharges from eight major inlets of the Pearl River system. Each inlet is approximated by a narrow (~7 km in the middle model and ~6 km in the inner model) and shallow (~2.5 m) channel in the model. The discharge from each inlet is specified in the term of the monthly-mean volume transport of river discharge at the head of the inlet. More information on the specification of river discharge in the model can be found in Tang *et al.* (2009) and Ji *et al.* (2011a).

The conventional one-way nesting technique (i.e., dynamic downscaling) is used in the nested-grid modelling system. Along the open boundary of the middle model, the surface elevations and depth-mean currents produced by the two-dimensional (2D) outer model are specified based on the open boundary condition of Davies & Flather (1978). For temperature and salinity variables at the open boundary of the middle model, the Orlanski (1976) radiation condition is first used to determine whether the open boundary is passive or active. If the open boundary is active, the model temperature and salinity at the open boundary are advected outward. If the open boundary is passive, the temperature and salinity at the open boundary are restored to the monthly mean climatology with a restoring time scale of 30 days. The same Orlanski (1976) radiation condition is also used at the open boundary of the inner model to determine whether the open boundary is passive or active. The model 3D currents and temperature/salinity at the open boundary of the inner model are advected outward if the open boundary is active. If the open boundary of the inner model is passive, the 3D currents and temperature/salinity produced by the middle model are used in specifying open boundary conditions of the inner model with a restoring time scale of 12 h. Finally, an additional barotropic adjustment is made to the depth-mean currents along the open boundary of the inner models based on the open boundary condition of Davies & Flather (1978) in order to have proper propagations of tidally and meteorologically forced surface elevations and depth-mean flows from the middle model to the inner model.

The model performance of the nested-grid modelling system was assessed by Tang *et al.* (2009) and Ji *et al.* (2011a) by comparing model results with *in-situ* and remote sensing observations including tidal gauge observations and surface and near-bottom salinity (NBS). In this study, the main focus is on the storm-induced circulation during Koryn over the PRE and adjacent waters. The nested-grid modelling system is integrated from the beginning of 1992 to the end of 1993. Model results from the two numerical experiments are presented in this paper. In the first numerical experiment (Run-Vortex), the nested-grid modelling system is forced with the suite of external forcing discussed above, including Holland's parameteric vortex presented in Equations (1)–(3). In the second experiment (Run-noVortex), the nested-grid model is forced by all the forcing functions except for the parameteric vortex. As mentioned earlier, the NMEFC atmospheric forcing has horizontal resolution of 0.5 °C which is too coarse to resolve the general structure of Koryn. Furthermore, the 3-hourly NMEFC fields are linearly interpolated to each model time step, and the interpolated NMEFC atmospheric forcing in the model does not represent well the rapid translation of the storm (Mecking *et al.* 2009). In comparison, Holland's parametric wind and pressure profiles are calculated at each model time step based on Equations (1)–(3) using the interpolated storm best track data. As a result, the differences of model results between the two experiments can be used to quantify the storm-induced circulation during Koryn.

MODEL RESULTS

Figure 4 represents a snapshot of simulated surface elevations and circulation produced by the nested-grid modelling system and wind stress at 00:00 June 26, 1993 (model day 542.0) in Run-Vortex. At this time, the vortex is centered at Luzon Island of the northern Philippines and the storm affects significantly circulation over coastal waters around the island. Outside the area influenced by the storm, the surface elevations and circulation produced by the outer model are driven mainly by the tides and large-scale atmospheric

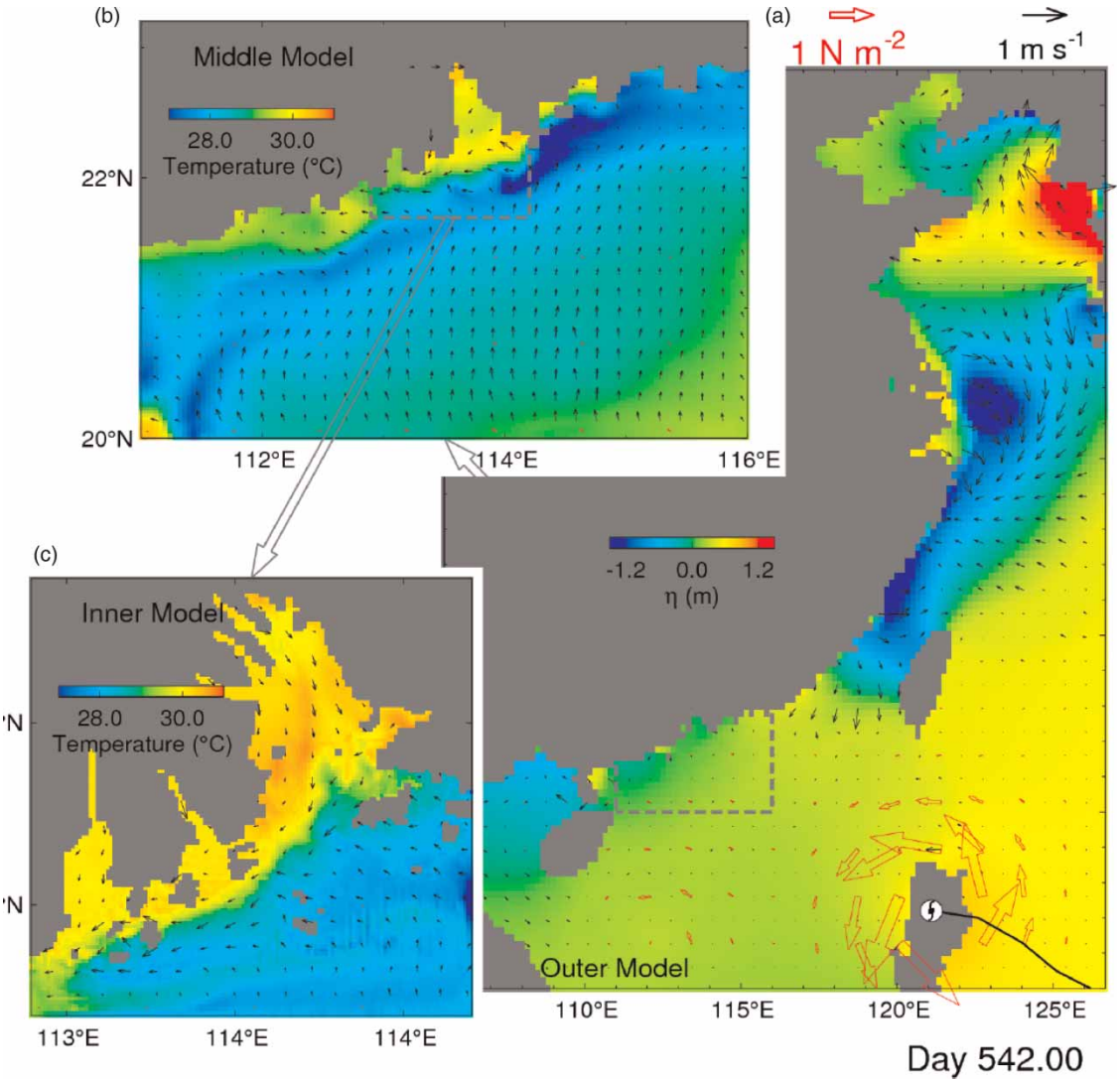

Figure 4 | Circulation at model day 542.0 (00:00 June 26, 1993) produced by the DalCoast-PRE in Run-Vortex. (a) Surface elevations (blue contours, in the unit of m) and depth-mean currents (solid black arrows) over China Seas produced by the outer model; (b) surface temperature (image) and surface currents (solid arrows) over the inner shelf of the northern South China Sea produced by the middle model; and (c) surface temperature (image) and surface currents (solid arrows) produced over the PRE produced by the inner model of the nested-grid system. Red open arrows represent wind stress vectors. Velocity vectors are plotted at every 10th grid point in (a) and every 6th grid point in (b) and (c). Please refer to the online version of this paper to see this figure in colour: http://www.iwaponline.com/wqrjc/toc.htm.

forcing (Figure 4(a)). The latter only plays a secondary role at this time. The sea surface temperature (SST) produced by the middle model (Figure 4(b)) in Run-Vortex features relatively uniform and about 29 °C in the deep waters over the inner shelf of the northern South China Sea, with cool strips over the inshore waters. The SST is about 30 °C inside the PRE, which is slightly warmer than the SST over the inner shelf (Figure 4(c)). The surface circulation at day 542.0 is relatively weak and mainly northward over the inner shelf and southward in the PRE.

Figure 5 presents evolutions of surface elevations and depth-mean currents produced by the outer model in Run-Vortex during a 3-day period from day 542.25 (06:00 June 26) to 545.25 (06:00 June 29) with a time interval of 24 h. During this period, the surface elevations and the depth-mean circulation in Run-Vortex are affected significantly by the vortex and tides over the northern South China Sea. Outside the area of influence of the storm, the surface elevations and depth-mean currents are driven primarily by tides during this period. At day 542.25, the

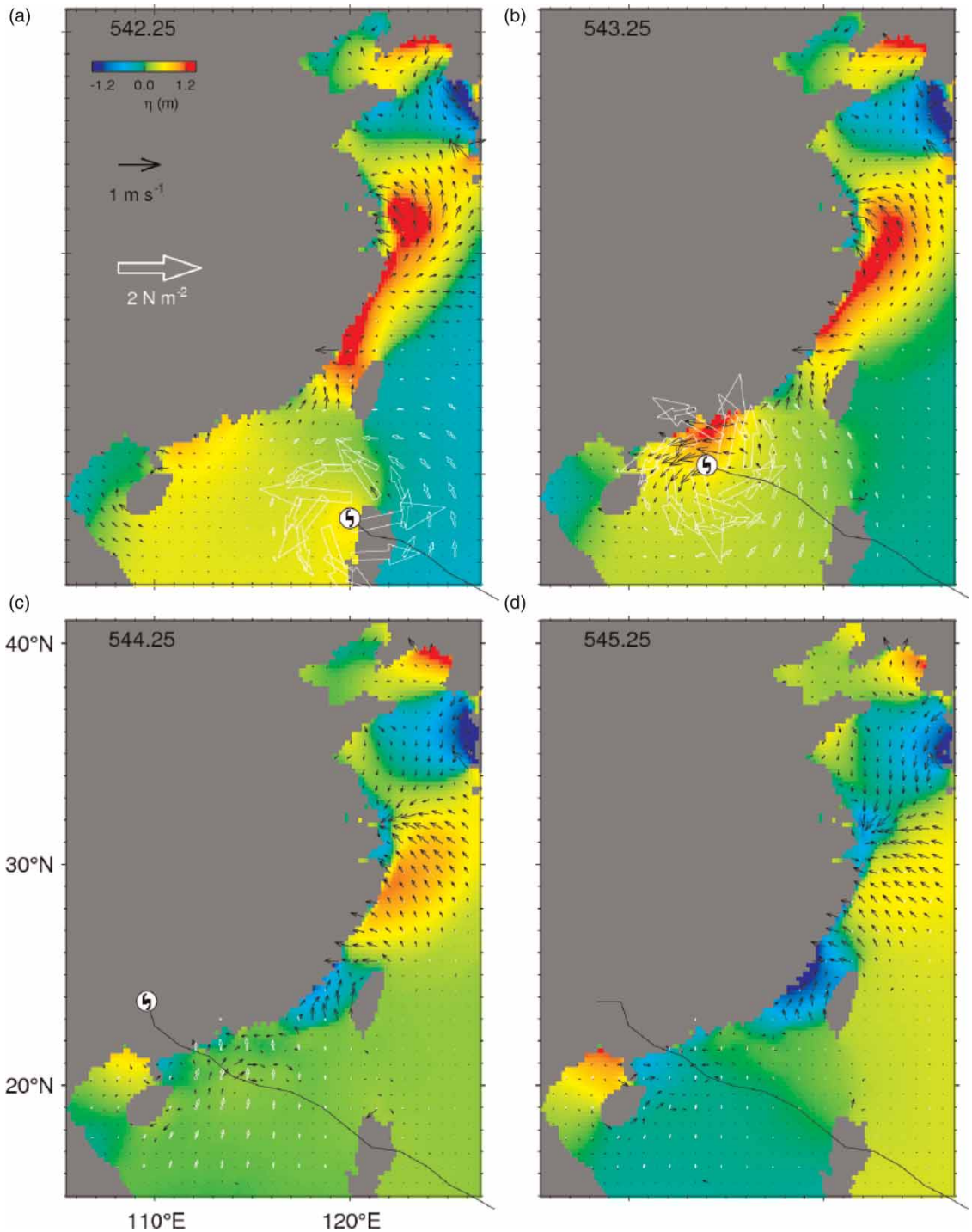

Figure 5 | Total sea surface elevations (image) and depth-mean currents (vectors) produced by the outer model in Run-Vortex at model day (a) 542.25 (06:00 June 26), (b) 543.25 (06:00 June 27), (c) 544.25 (06:00 June 28) and (d) 545.25 (06:00 June 29). The solid line represents the best storm track of Koryn. Velocity vectors are plotted at every 10th grid point.

storm center is located over the coastal waters to northwestern Luzon Island, and the outer model generates positive sea surface elevations (positive surge) over the areas influenced directed by the storm (Figure 5(a)). It should be noted that the surface elevations shown in Figure 5 are total sea surface elevations which include components

driven by tides and wind forcing and the inverted barometer effect. The last component is important over the area of influence of the storm due to large changes of atmospheric pressures inside the storm (a sea level rise of 10 cm for a drop of atmospheric pressure of 1 kPa). About 24 h later at day 543.25, the center of the vortex is located at about 20 km south of the PRE, and a positive surge is generated over the inner shelf waters outside the PRE due to the combination of strong onshore wind forcing and a drop of the atmospheric pressure associated with the vortex (Figure 5(b)). This positive surge propagates southwestward along the coast and then gradually dissipates (Figures 5(c),(d)). In comparison, the model-calculated sea surface elevations and depth-mean currents in Run-noVortex (Figure 6) do not have large surface elevations and strong depth-mean currents over the areas affected directly by Koryn, indicating again that the NMEFC atmospheric forcing alone is not enough to produce storm-induced surges and strong coastal currents over the inner shelf of the northern South China Sea during Koryn.

To quantify the changes of hydrodynamics associated with super Typhoon Koryn over the inner shelf of the northern South China Sea, the differences between the model results in Run-Vortex and Run-noVortex are used to represent the storm-induced changes in oceanographic conditions in the study region. Figure 7 presents changes of sea surface elevations ($\Delta\eta$) associated with the parametric vortex produced by the outer model over the northern South China Sea from day 542.25 to 544.75. The parametric vortex is responsible for generating positive sea surface elevations that propagate northwestward with the storm before the storm reaches the coastal waters near the PRE (Figures 7(a),(b)). During this period (days 542.25–544.75), the positive surface elevations under the storm are associated mainly with the inverted barometer effect. At day 543.25 (Figure 7(c)), a large positive surge occurs over the coastal area between the storm center and the PRE, due to the combination of sea level setup introduced by the onshore wind and positive surface elevations associated with the inverted barometer effect. At day 543.75 (Figure 7(d)), a large positive surge occurs near the coastal waters off the PRE and negative surges occur over coastal waters to the north of the PRE and further west of the PRE. The storm surge dissipates after day 544.25 (Figures 7(e),(f)).

Figure 8 presents the changes of SST associated with the vortex produced by the middle model. The storm-induced SST changes are relatively small over the middle model domain before day 543.00. At day 543.25 as the vortex center is located at about 200 km to south of the PRE, the storm-induced SST cooling of about 3 °C occurs in the radius of approximately 150 km around the storm center (Figure 8(c)). Outside this area of influence and over the areas close to the shore, the storm-induced SST changes are small. As demonstrated by Price (1981), Zhai *et al.* (2004) and Sheng *et al.* (2006), the intense SST cooling along the track of the storm is generated by strong vertical mixing associated with the intense wind forcing of the storm, and the vertical advection term only plays a secondary role. At day 543.50 the vortex center is located at about 50 km from the coast to southwest of the PRE (Figure 8(d)). The vortex has made landfall by day 543.75. The strength of the SST cooling reaches strongest at day 543.75 (Figure 8(e)) and then dissipates gradually with time (Figure 8(f)).

We next examine the storm-induced changes of sea surface salinity (SSS) in the PRE and adjacent waters produced by the inner model (Figure 9). The storm-induced SSS changes are small before day 542.75, but large from day 543.0 to 544.0 over the outer PRE where a sharp salinity front occurs in the summer wet months due to large freshwater runoff from the Pearl River (Tang *et al.* 2009; Ji *et al.* 2011a, b). The intense landward (northwestward) storm-induced currents in the surface layer of the outer PRE (Figures 9(b),(d)) push the salinity front landward, which explains why large SSS changes of greater than 8 psu occur during the period from day 543.0 to 543.75 (Figures 9(b)–(e)). After the landfall of the storm, the SSS changes are relatively small (Figure 9(f)) due to the fact that the storm-induced surface currents over the outer PRE are seaward (southeastward) associated with the relaxation of pressure gradients that were generated earlier by the storm which bring the surface salinity front to its normal condition.

Large storm-induced changes also occur in the NBS over the outer PRE and adjacent waters (Figure 10). Similar to the large SSS changes, the large and positive NBS changes of about 8 psu are due mainly to the landward movements of the salinity front driven by the onshore currents associated with the storm (Figures 10(b),(c)). At day

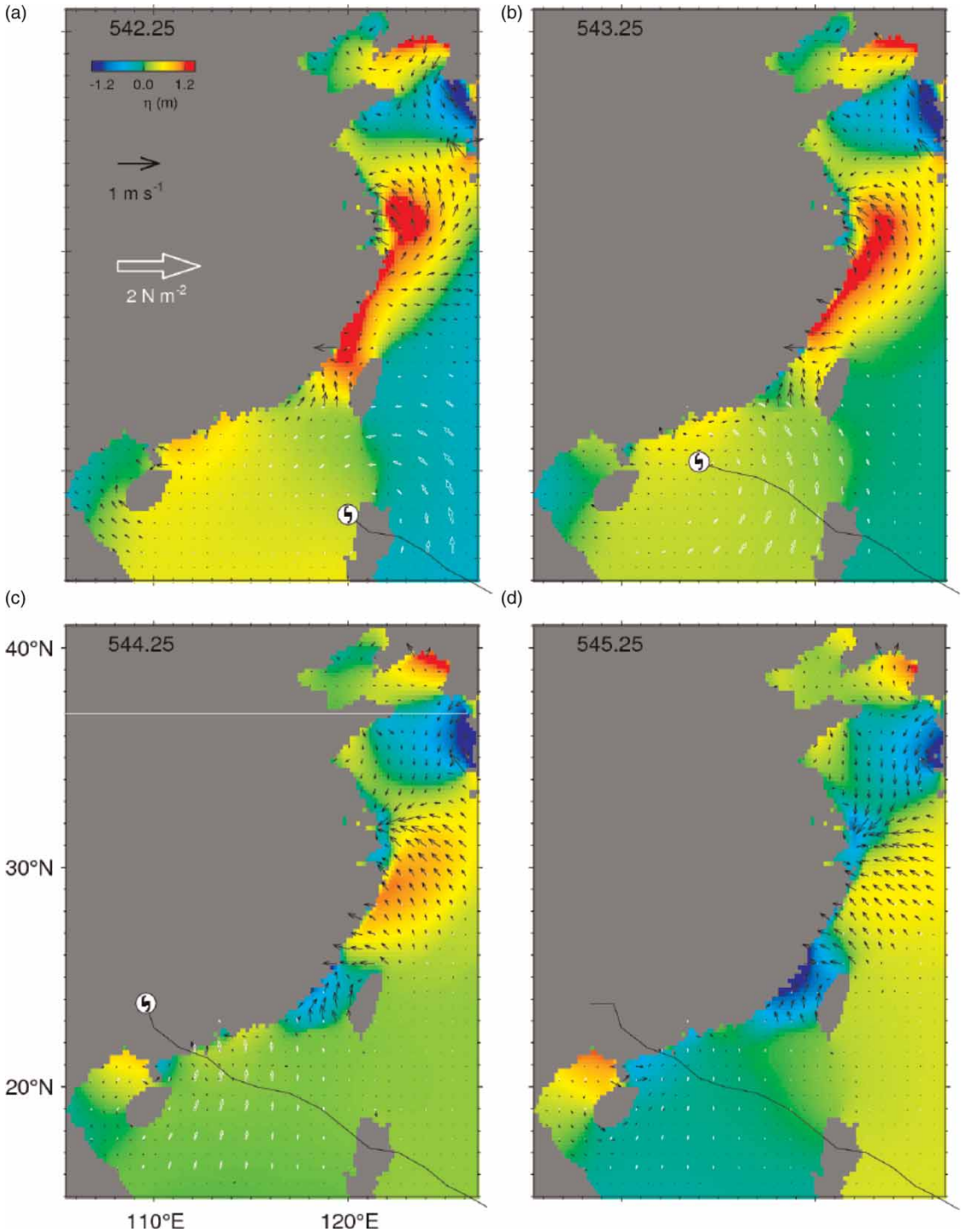

Figure 6 | Total sea surface elevations (image) and depth-mean currents (vectors) produced by the outer model in Run-NoVortex at model day (a) 542.25 (06:00 June 26), (b) 543.25 (06:00 June 27), (c) 544.25 (06:00 June 28) and (d) 545.25 (06:00 June 29). The solid line represents the best storm track of Koryn. Velocity vectors are plotted at every 10th grid point.

543.75, the storm wind has diminished and the near-surface currents are seaward over the outer PRE. The strong seaward currents bring the NBS front seaward and reduce the storm-induced NBS changes (Figures 10(e),(f)).

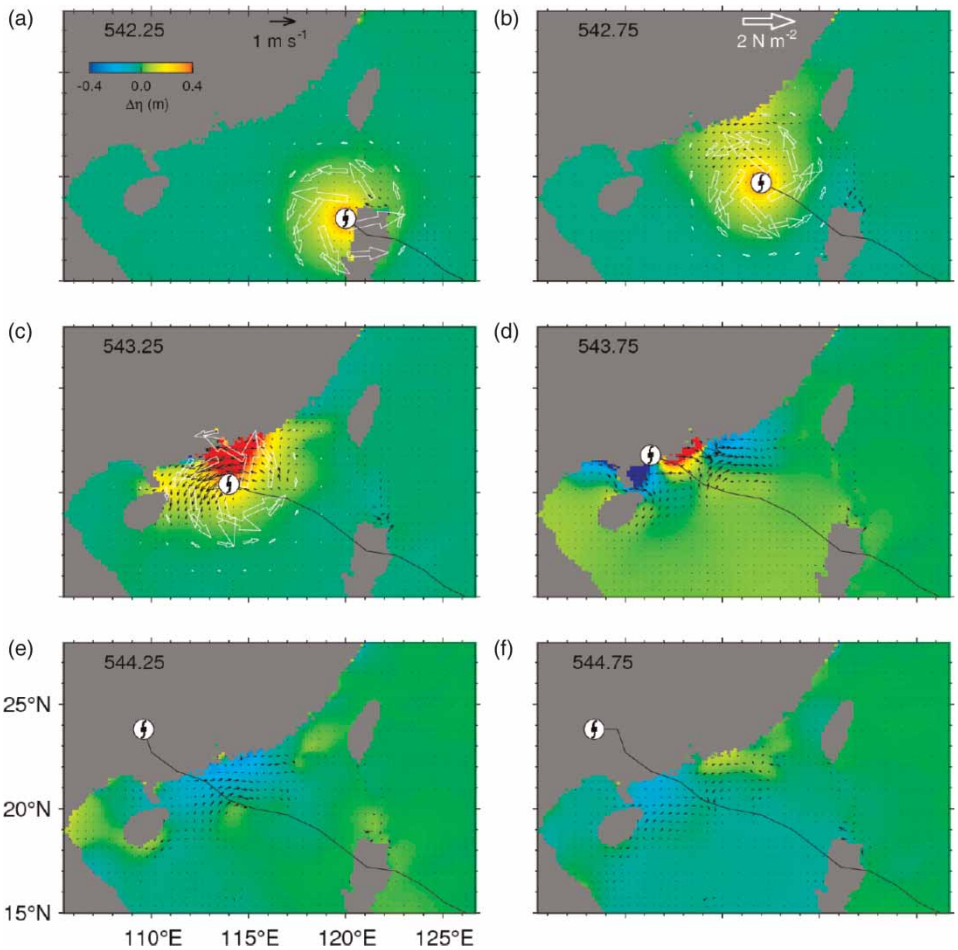

Figure 7 | Changes of total sea surface elevations (image) and depth-mean currents (vectors) associated with Typhoon Koryn produced by the outer model at day (a) 542.25 (06:00 June 26), (b) 542.75 (18:00 June 26), (c) 543.25 (06:00 June 27), (d) 543.75 (18:00 June 27), (e) 544.25 (06:00 June 28), and (f) 544.75 (18:00 June 28). Velocity vectors are plotted at every 10th grid point.

One of important issues for water quality management is how to accurately predict the movements and dispersion of pollutants in the water under different environmental conditions. In this study, we examine the horizontal movements of near-surface particles during Koryn in order to gain a better understanding of the effect of storm-induced currents on the particle movements. The 3D movements of particles carried passively by ocean currents are calculated using the fourth-order Runge-Kutta method (Press *et al*. 1990):

$$\vec{x}(t_0 + \Delta t) = \vec{x}(t_0) + \int_{t_0}^{t+\Delta t} \vec{u}(\vec{x}, t)\, \mathrm{d}t + \vec{\delta} \tag{4}$$

where $\vec{x}(t_0 + \Delta t)$ and $\vec{x}(t_0)$ are 3D position vectors of a passive particle at time $t_0 + \Delta t$ and initial time t_0, respectively, $\vec{u}(\vec{x}, t)$ is the 3D velocity vector of model currents, and $\vec{\delta}$ is additional random horizontal displacements used to represent the influence of physical processes (Sheng *et al*. 2009b) that are not modelled explicitly in this study and is expressed as

$$\vec{\delta} = (\xi\sqrt{2\kappa\Delta t}, \varsigma\sqrt{2\kappa\Delta t}) \tag{5}$$

where ξ and ζ are random deviations from a Gaussian distribution of zero mean and unit variance, respectively, Δt (2 h) is the time step used in the numerical integration, which is much greater than the time steps used in the numerical simulation of the nested-grid modelling system, and κ is a horizontal eddy diffusivity for the random displacements which is set to 4 $\mathrm{m^2\,s^{-1}}$.

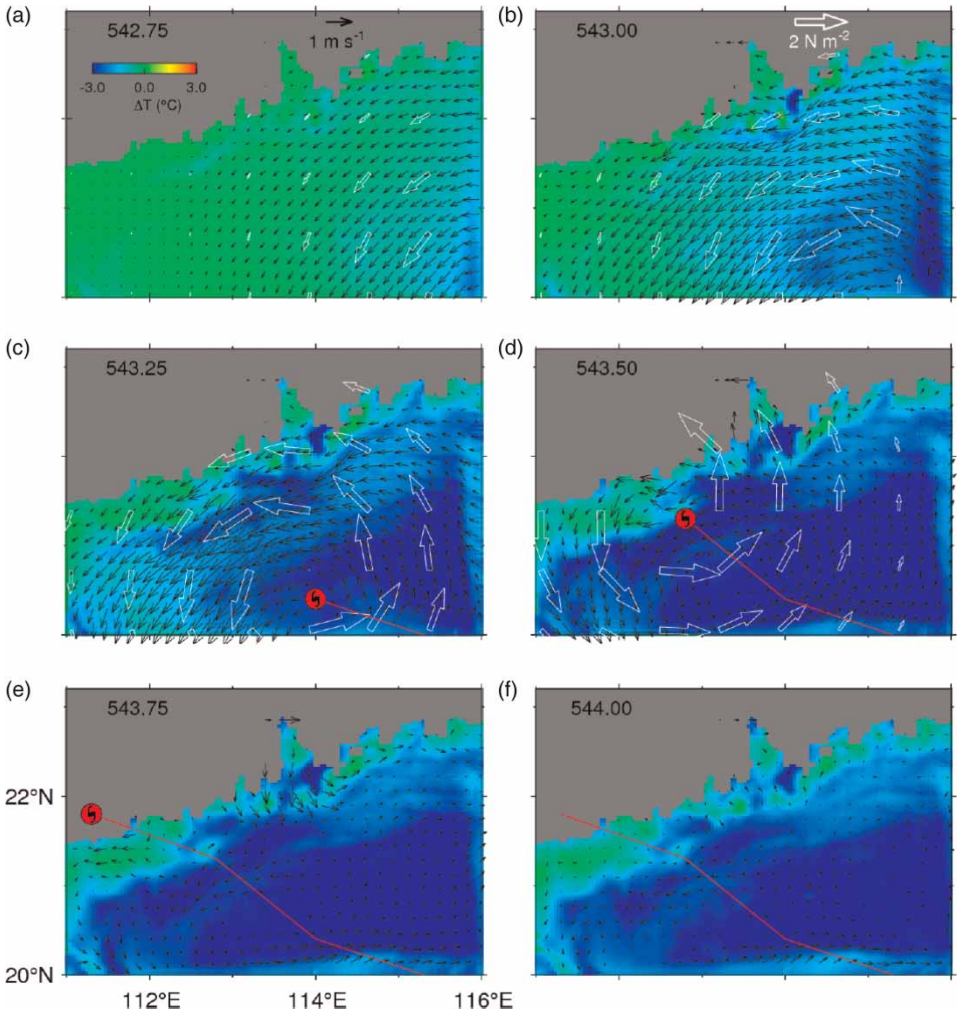

Figure 8 | Changes of seas surface temperature (image) and surface currents (vectors) associated with typhoon Koryn produced by the middle model at day (a) 542.75 (18:00 June 26), (b) 543.0 (00:00 June 27), (c) 543.25 (06:00 June 27), (d) 543.50 (12:00 June 27), (e) 543.75 (18:00 June 27), and (f) 544.0 (00:00 June 28). Velocity vectors are plotted at every 6th grid point.

The horizontal trajectories of particles in the surface layer of less 4 m over the inner shelf waters off the PRE (i.e., the middle model domain) during 24 h in Run-noVortex and Run-Vortex are shown in Figures 11 and 12, respectively. The 24-h trajectories are calculated using the 2-hourly currents produced by the middle model in each experiment. Comparison of the 24-h trajectories in the two experiments demonstrates the important role of the storm-induced currents in the movements and dispersion of near-surface particles over the region. At day 542.79, the horizontal movements of near-surface particles over the shallow coastal areas with water depths less than 60 m of the middle model domain are affected mainly by the tidal currents and the large-scale southwestward shelf circulation. The movements of near-surface particles at this time are characterized by relatively small and southwestward horizontal displacements over coastal waters off the PRE and relatively large and southward displacements over the coastal waters to the northeast of Hainan Island (Figures 11(a) and 12(a)). In the deep water region with water depths greater than 60 m to the southwest of the PRE, there are large differences in the 24-h trajectories of the near-surface particles between these two experiments. In Run-noVortex, the near-surface particles over the deep water region move first northward and then change to westward in the 24-h period (Figure 11(a)), due to the combination of tidal currents and shelf circulation forced by

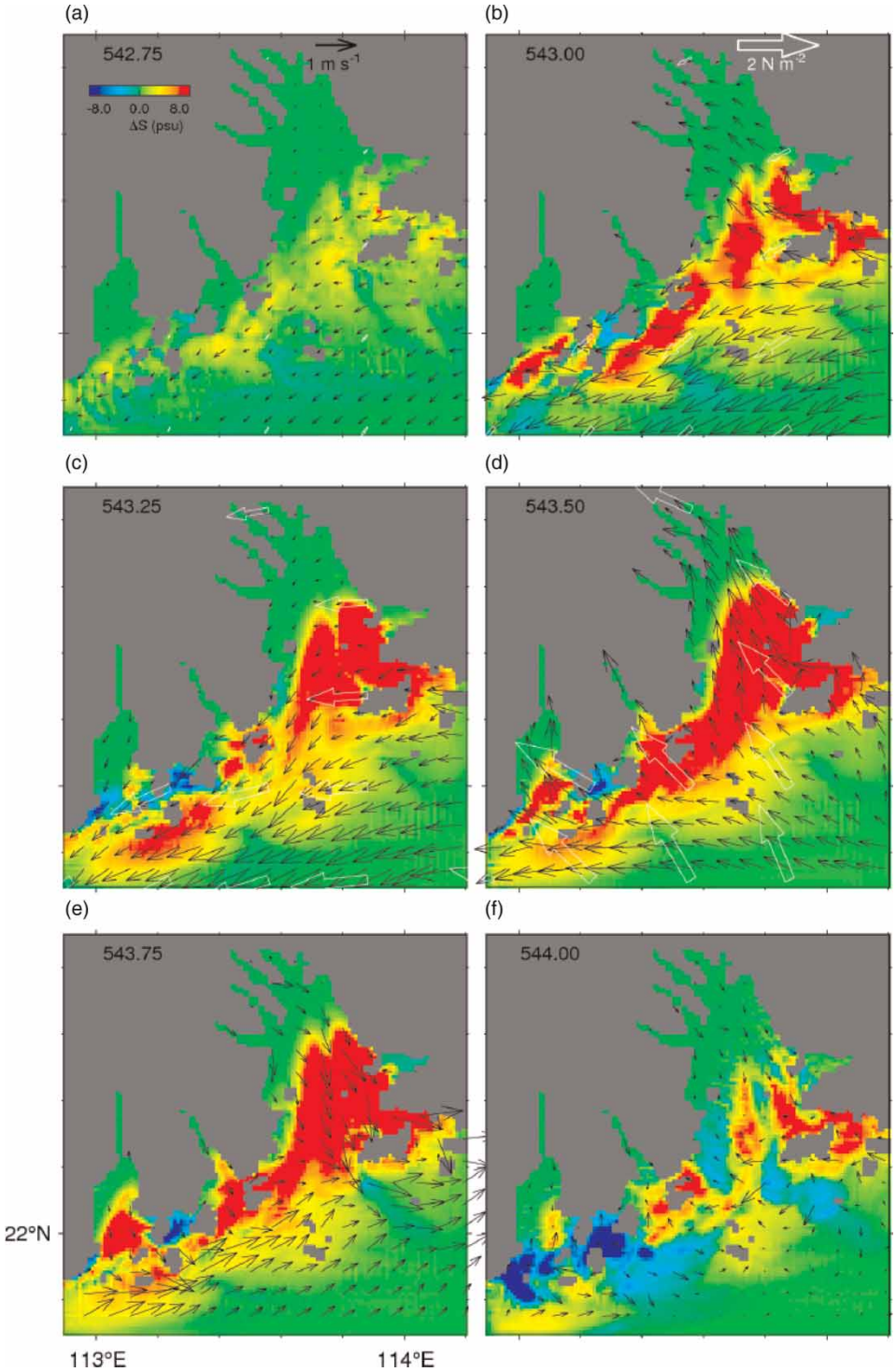

Figure 9 | Changes of seas surface salinity (image) and surface currents (vectors) associated with Typhoon Koryn produced by the inner model at day (a) 542.75 (18:00 June 26), (b) 543.0 (00:00 June 27), (c) 543.25 (06:00 June 27), (d) 543.50 (12:00 June 27), (e) 543.75 (18:00 June 27), and (f) 544.0 (00:00 June 28). Velocity vectors are plotted at every 6th grid point.

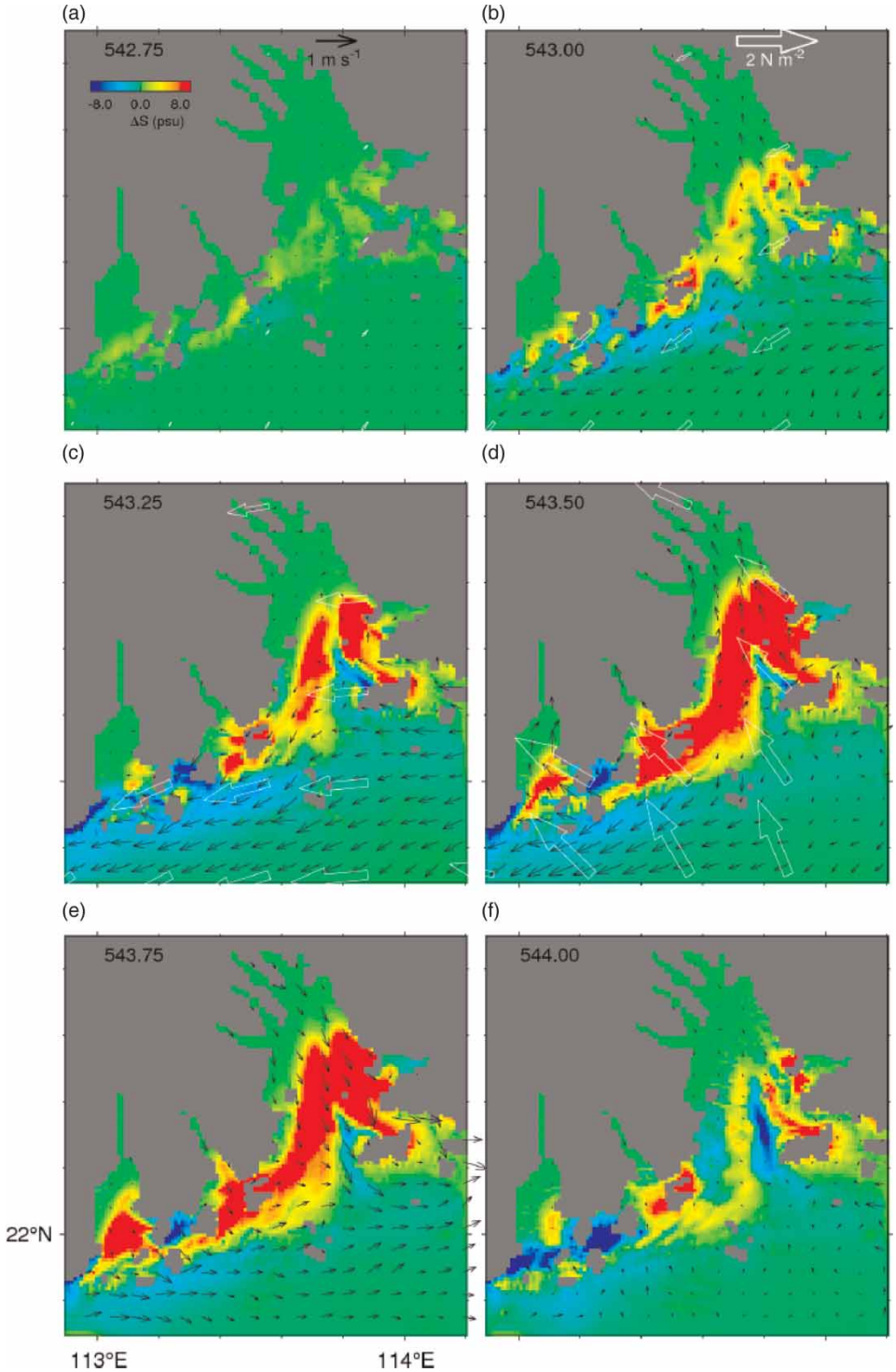

Figure 10 | Changes of bottom salinity (image) and surface currents (vectors) associated with Typhoon Koryn produced by the inner model at day (a) 542.75 (18:00 June 26), (b) 543.0 (00:00 June 27), (c) 543.25 (06:00 June 27), (d) 543.50 (12:00 June 27), (e) 543.75 (18:00 June 27), and (f) 544.0 (00:00 June 28). Velocity vectors are plotted at every 6th grid point.

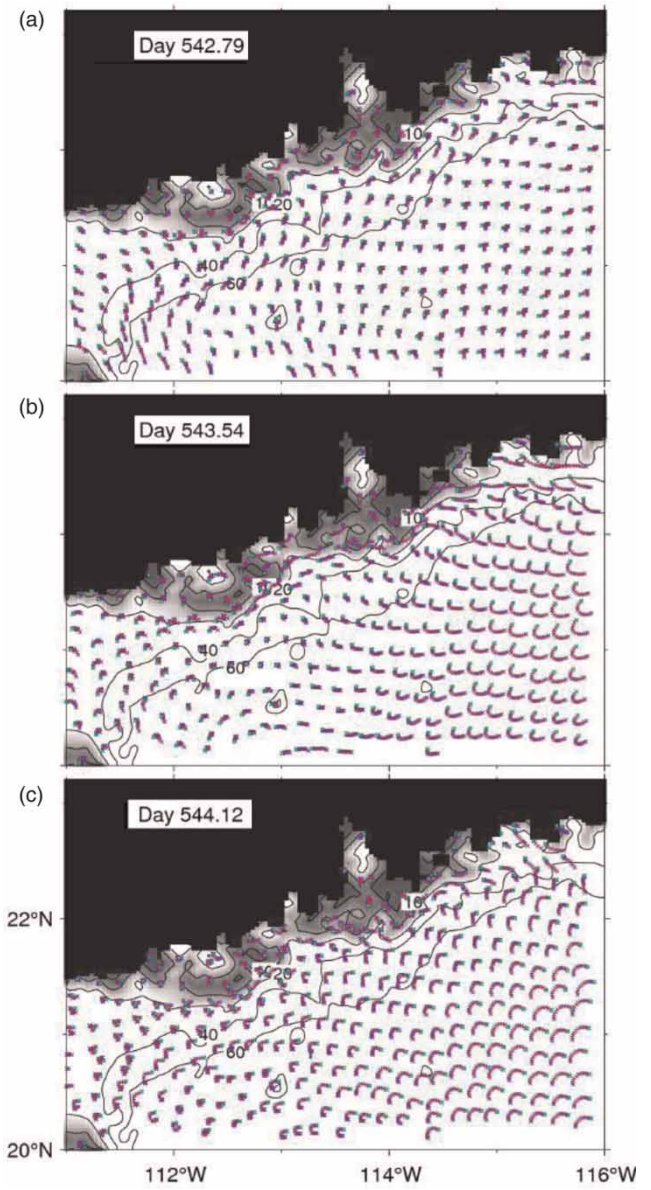

Figure 11 | 24-h trajectories of surface particles carried by currents produced the middle model in Run-noVortex at day (a) 542.79, (b) 543.54, and (c) 544.12. The green dot represents the current position and the red line represents trajectories in the past 24 h. The green symbol marks time interval of 2 h. Please refer to the online version of this paper to see this figure in colour: http://www.iwaponline.com/wqrjc/toc.htm.

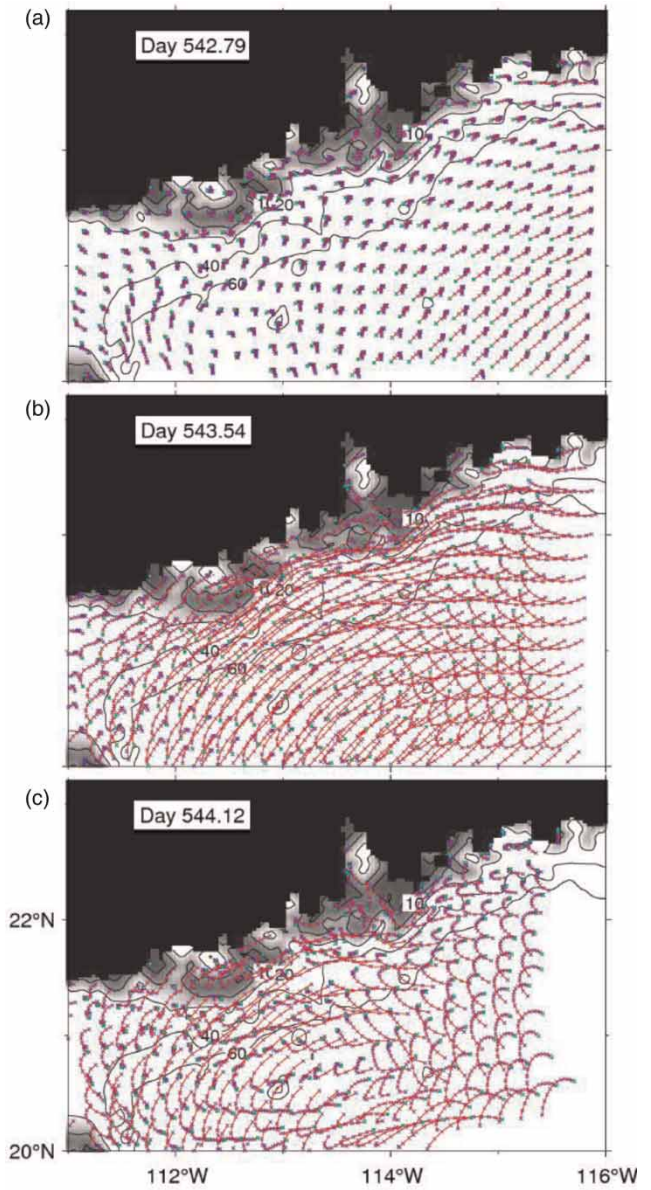

Figure 12 | 24-h trajectories of surface particles carried by currents produced the middle model in Run-Vortex at day (a) 542.79, (b) 543.54, and (c) 544.12. The green dot represents the current position and the red line represents trajectories in the past 24 h. The green symbol marks time interval of 2 h. Please refer to the online version of this paper to see this figure in colour: http://www.iwaponline.com/wqrjc/toc.htm.

the large-scale atmospheric forcing. By comparison, in Run-Vortex, the 24-h trajectories of near-surface particles in the deep water region at day 542.79 have small northward displacements first and then large southwestward displacements (Figure 12(a)), demonstrating the effect of the storm-induced currents on the movements of near-surface particles.

At day 543.54, the 24-h trajectories of near-surface particles in Run-noVortex also feature equator ward displacements in the shallow water areas and relatively large and clockwise displacements in the deep water region over the middle model domain (Figure 11(b)). By comparison, the 24-h trajectories of near-surface particles in

Run-Vortex at this time (Figure 12(b)) have large southeastward displacements (about 40–80 km in 24 h) over the shallow water areas near the coast and clockwise (anticyclonic) displacements in the deep water region to the south of the PRE due to the intense storm-induced currents.

The near-surface particles in Run-noVortex at day 544.12 (Figure 11(c)) have horizontal movements very similar to those at day 543.54, particularly in the deep water region of the middle model domain. By comparison, in Run-Vortex, the movements of the near-surface particles at this time (Figure 12(c)) have large equator ward movements in the shallow waters and moderate clockwise displacements in the deep water region affected by the storm. Figure 12(c) also shows that trajectories of near-surface particles at day 544.12 have large spatial variability associated with the storm.

To further examine the movements of near-surface particles inside the PRE and adjacent waters, the 2-hourly currents produced by the inner model of the nested-grid modelling system are used in tracking trajectories of the particles. The inner model has a fine spatial resolution of ~1.2 km and resolves better the 3D circulation in the PRE than the middle model (~3 km). The 10-h trajectories of near-surface particles in the PRE and adjacent waters in Run-noVortex and Run-Vortex are presented in Figures 13 and 14, respectively. The 10-h trajectories of the near-surface particles inside the PRE at day 542.75 in Run-noVortex have gradual seaward displacements superposed by rectilinear displacements. The gradual seaward displacements of near-surface particles in the PRE are associated with the density-driven estuarine circulation in the PRE. Under the normal calm condition in summer wet months (Ji *et al.* 2011a), the density-driven estuarine circulation in the PRE is characterized by a strong seaward flow of about 10 cm s^{-1} in the top 5 m and relatively weaker and landward currents at depths greater than 5 m (Ji *et al.* 2011a, b). In addition, there is a northeastward coastal current along the coast of the inner shelf waters off the PRE in the normal summer months (Ji *et al.* 2011a, b). Due to the influence of the large-scale atmospheric forcing during Koryn, however, the coastal current reverses its normal direction to flow southwestward (Figures 8(a)–(c)). The 10-h trajectories of near-surface particles in Run-Vortex are very similar to Run-noVortex at day 542.75, except for the near-surface

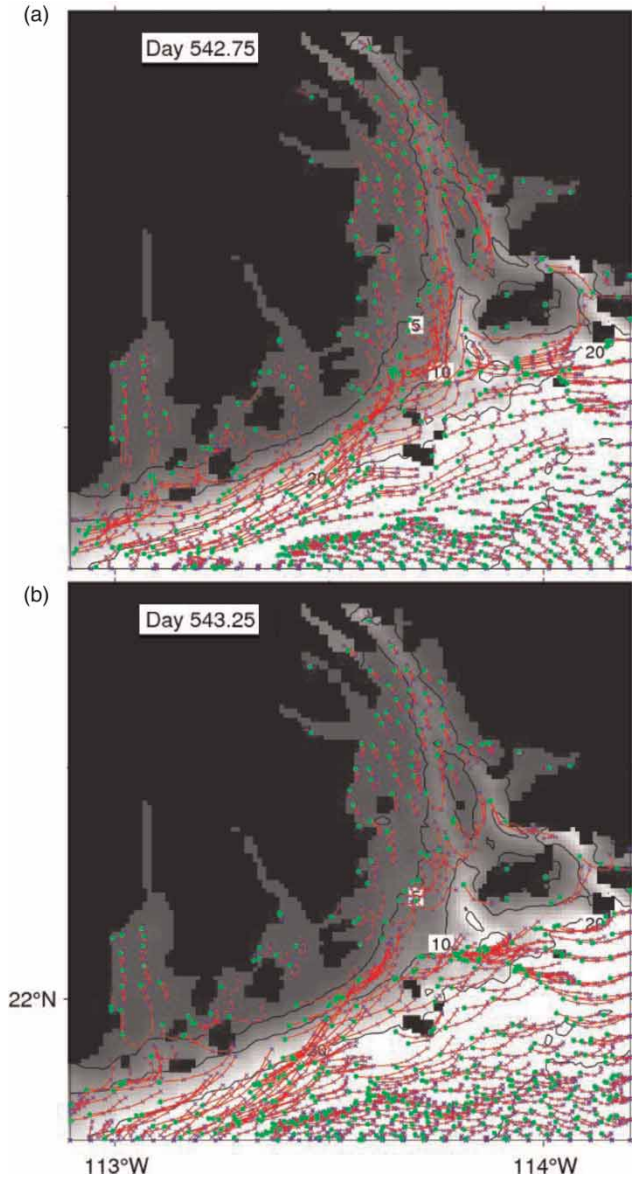

Figure 13 | 10-h trajectories of surface particles carried by currents produced the inner model in Run-noVortex at day (a) 542.75, and (b) 543.25. The green dot represents the current position and the red line represents trajectories in the past 10 h. The green symbol marks the time interval of 2 h. Please refer to the online version of this paper to see this figure in colour: http://www.iwaponline.com/wqrjc/toc.htm.

particles over the offshore area to the south of the outer PRE. Over this offshore area, the near-surface particles in Run-Vortex have large southwestward displacements due to the strong southwestward currents induced by the storm.

Figure 13 demonstrates that the 10-h trajectories of the near-surface particles at day 543.25 are very similar to

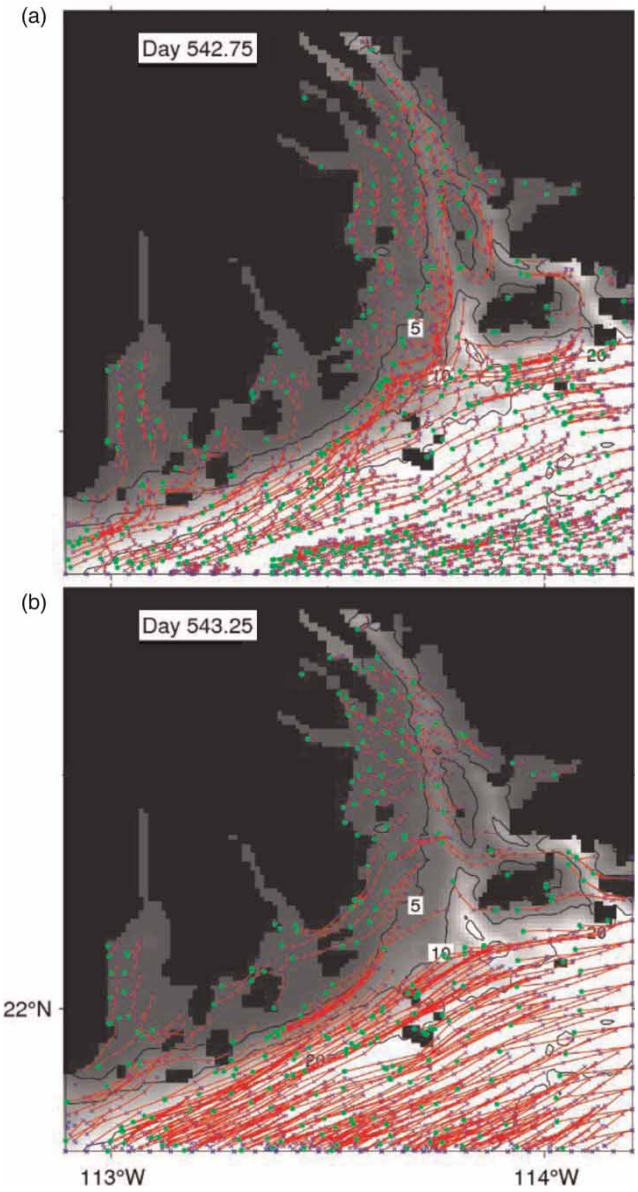

Figure 14 | 10-h trajectories of surface particles carried by currents produced the inner model in Run-Vortex at day (a) 542.75, and (b) 543.25. The green dot represents the current position and the red line represents trajectories in the past 10 h. The green symbol marks time interval of 2 h. Please refer to the online version of this paper to see this figure in colour: http://www.iwaponline.com/wqrjc/toc.htm.

these at day 542.75 in Run-noVortex, with near-surface particle movements affected by oscillatory tidal currents and the seaward estuarine near-surface circulation inside the PRE and nearly westward movements in the offshore area off the outer PRE due to the equator ward coastal current. By comparison, the near-surface particles in Run-Vortex have significant large displacements at this time, with large southwestward displacements in the offshore area off the PRE and westward displacements inside the PRE.

CONCLUSIONS AND DISCUSSION

Circulation and hydrography over many coastal and shelf waters are affected significantly by hurricanes and tropical and winter storms. For example, Atlantic Canada was struck by Hurricane Juan, which made landfall on the south coast of Nova Scotia near Halifax on September 29, 2003 as a category-2 hurricane. Previous studies demonstrated that tropical storms and hurricane frequencies vary considerably from year to year, with substantial increases in storm intensity and duration since the 1970s (IPCC 2007). Better knowledge of storm-induced changes in hydrodynamics will help for more accurate predictions of circulation and movements of particles in the water. In this study, the storm-induced changes in circulation and hydrography in the PRE and adjacent waters of the South China Sea during super Typhoon Koryn in June 1993 were investigated based on numerical results produced by a nested-grid ocean circulation modelling system. The model forcing used in this study includes tides, freshwater runoff from the Pearl River, sea surface heat and freshwater fluxes, wind stress and atmospheric pressure fields at the sea level. To better represent the atmospheric pressure and wind profiles inside Koryn, a parametric vortex suggested by Holland (1980) was inserted into the coarse-resolution (0.5°) numerical weather forecast products provided by the National Environmental Forecast Center of China (NMEFC). Analysis of model results demonstrates that large positive storm surges (due mainly to the inverse barometer effect) were generated over the area of influence of the storm when the storm is in the deep water far from the PRE. As the storm reached the coast, the wind-induced setup also contributed to the total storm surge. Due to the constraint of the coastline and the effect of the Earth's rotation, the storm surge near the coast excited the coastal trapped waves that propagated equatorward along the coast (on the north hemisphere). The storm also introduced large cooling of the SST due mainly to the intense vertical mixing induced by the storm. The storm also introduced large changes in the salinity fields over the outer PRE and

significant movements and dispersion of near-surface particles in the PRE and adjacent inner shelf waters.

ACKNOWLEDGMENTS

The authors wish to thank Xiaomei Ji, Dabin Liu, Qinzheng Liu, Fujiang Yu, Xuelian Yang, Chonghao Wang, Keith Thompson, Kyoko Ohashi, Yueheng Tseng, and two anonymous reviewers for their comments and suggestions. This study is part of Hydrological Simulation & Regulation of Watersheds supported by National Natural Science Foundation of China (51021006), and supported by China Institute of Water Resources and Hydropower Research Foundation (NJ1029) and Natural Sciences and Engineering Research Council of Canada and The Lloyd's Register Educational Trust (The LRET). The LRET is an independent charity working to achieve advances in transportation, science, engineering and technology education, training and research worldwide for the benefit of all.

REFERENCES

Davies, A. M. & Flather, R. A. 1978 Computing extreme meteorologically induced currents, with application to the northwest European continental shelf. *Cont. Shelf Res.* **7**, 643–683.

Gan, J., Li, L., Wang, D. & Guo, X. 2009 Interaction of a river plume with coastal upwelling in the north eastern South China Sea. *Cont. Shelf Res.* **29**, 728–740.

Gill, A. E. 1982 *Atmosphere-Ocean Dynamics*. Academic, San Diego, pp. 662.

Harrison, P. J., Yin, K., Leed, J., Gan, J. & Liu, H. 2008 Physical–biological coupling in the Pearl River Estuary. *Cont. Shelf Res.* **28**, 1405–1415.

Holland, G. 1980 An analytic model of the wind and pressure profiles in hurricanes. *Mon. Weather Rev.* **108**, 1212–1218.

Huang, Z., Zong, Y. & Zhang, W. 2004 Coastal inundation due to sea level rise in the Pearl River Delta, China. *Natural Hazards* **33**, 247–264.

IPCC 2007 Climate Change 2007: The Physical Science Basis. *Contribution of Working Group I to the Fourth Assessment Report of the Intergovernmental Panel on Climate Change* (S. Solomon, D. Qin, M. Manning, Z. Chen, M. Marquis, K. B. Averyt, M. Tignor & H. L. Miller, eds). Cambridge University Press, Cambridge, UK and New York, NY, USA.

Ji, X., Sheng, J., Tang, L., Liu, D. & Yang, X. 2011a Process study of circulation in the Pearl River Estuary and adjacent coastal waters in the wet season using a triply-nested coastal circulation model. *Ocean Mod.* **38**, 138–160.

Ji, X., Sheng, J., Tang, L., Liu, D. & Yang, X. 2011b Process study of dry-season circulation in the Pearl River Estuary and adjacent coastal waters using a triple-nested coastal circulation model. *Atm. Ocean* **49**, 138–162.

Larson, M., Bellanca, R., Jonsson, L., Chen, C. & Shi, P. 2005 A model of the 3D circulation, salinity distributions, and transport patterns in the Pearl River Estuary, China. *J. Coast Res.* **21**, 896–908.

Matsumoto, K., Sato, T., Takanezawa, T. & Ooe, M. 2001 GOTIC2: a programme for computation of oceanic tidal loading effect. *J. Geo. Soc. Jpn.* **47**, 243–248.

Mecking, J., Fogarty, C.T., Greatbatch, R. J., Sheng, J. & Mercer, D. 2009 Using atmospheric model ouput to simulate the meteorological tsunami response to Tropical Storm Helene (2000). *J. Geophys. Res.* **114**, C10005.

Mellor, G. L. 2004 Users guide for a three-dimensional, primitive equation, numerical ocean model. Progress of Atmosphere and Ocean Sciences, Princeton University, 53 pp.

Orlanski, I. 1976 A simple boundary condition for unbounded hyperbolic flows. *J. Comput. Phys.* **21**, 251–269.

Press, W. H., Flannery, B. P., Teukolsky, S. A. & Vetterling, W. T. 1990 *Numerical Recipes*. Cambridge University Press, Cambridge, 702 pp.

Price, J. F. 1981 Upper ocean response to a hurricane. *J. Phys. Oceanogr.* **11**, 153–175.

Sheng, J., Tang, L., Cao, W., Yang, B. & Liu, D. 2009a Development and application of nested-grid coastal circulation models. *Proceedings of Academic Forum on Water Resources and Hydropower*, Beijing, China, pp. 146–163 (in Chinese).

Sheng, J., Zhao, J. & Zhai, L. 2009b Examination of circulation, dispersion, and retention in Lunenburg Bay of Nova Scotia using a nested-grid circulation model. *J. Mar. Sys.* **77**, 350–365.

Sheng, J., Zhai, X. & Greatbach, R. J. 2006 Numerical study of the storm-induced circulation on the Scotia shelf during Hurricane Juan using a nested-grid ocean model. *Progr. Oceanogr.* **70**, 233–254.

Song, L. 2003 Numerical forecasts of typhoon-induced surges over coastal waters of east coast of Guangdong. *Mar. Forecasts* **20**, 70–75 (in Chinese).

Tang, L., Sheng, J., Ji, X., Cao, W. & Liu, D. 2009 Investigation of circulation and hydrography over the Pearl River Estuary of China using a nested-grid coastal circulation model. *Ocean Dyn.* **59**, 899–919.

Wang, S., Tang, D., He, F., Fukuuo, Y. & Azanza, R. 2008 Occurrences of harmful algal blooms (HABS) associated with ocean environments in the South China Sea. *Hydrobiologia* **596**, 79–93.

Wong, L., Chen, J., Xue, H., Dong, L., Guan, W. & Su, J. 2003b A model study of the circulation in the Pearl River

Estuary (PRE) and its adjacent coastal waters: 2. Sensitivity experiments. *J. Geophys. Res.* **108**, C3157.

Wong, L., Chen, J., Xue, H., Dong, L., Su, J. & Heinke, G. 2003a A model study of the circulation in the Pearl River Estuary (PRE) and its adjacent coastal waters: 1. Simulations and comparison with observations. *J. Geophys. Res.* **108**, C3156.

Zhai, X., Greatbatch, R. J. & Sheng, J. 2004 Advective spreading of storm-induced inertial oscillations in a model of the northwest Atlantic Ocean. *Geophys. Res. Lett.* **31**, L14315.

Zhao, H., Tang, D. & Wang, D. 2009 Phytoplankton blooms near the Pearl River Estuary induced by Typhoon Nuri. *J. Geophys. Res.* **114**, C12027.

First received 18 February 2012; accepted in revised form 23 May 2012